symmetry

MDPI

Article

Concrete Based Jeffrey Nanofluid Containing Zinc Oxide Nanostructures: Application in Cement Industry

Nadeem Ahmad Sheikh [1,2], Dennis Ling Chuan Ching [1], Ilyas Khan [3,*], Afnan Ahmad [4] and Syed Ammad [4]

1 Fundamental and Applied Science Department, Universiti Teknologi PETRONAS, Perak 32610, Malaysia; mathwise1990@gmail.com (N.A.S.); dennis.ling@utp.edu.my (D.L.C.C.)
2 Department of Mathematics, City University of Science and Information Technology, Peshawar 25000, Pakistan
3 Faculty of Mathematics and Statistics, Ton Duc Thang University, Ho Chi Minh City 72915, Vietnam
4 Civil and Environmental Engineering Department, Universiti Teknologi PETRONAS, Perak 32610, Malaysia; afnan_19001642@utp.edu.my (A.A.); syed_18003311@utp.edu.my (S.A.)
* Correspondence: ilyaskhan@tdtu.edu.vn

Received: 19 March 2020; Accepted: 3 April 2020; Published: 20 June 2020

Abstract: Concrete is a non-Newtonian fluid which is a counterexample of Jeffrey fluid. The flow of Jeffrey fluid is considered containing nanostructures of zinc oxide in this study. The flow of the nanofluid is modeled in terms of partial fractional differential equations via Atangana–Baleanu (AB) fractional derivative approach and then solved using the integral transformation. Specifically, the applications are discussed in the field of concrete and cement industry. The variations in heat transfer rate and skin friction have been observed for different values of volume fractions of nanoparticles. The results show that by adding 4% ZnO nanoparticles increase skin friction up to 15%, ultimately enhancing the adhesion capacity of concrete. Moreover, ZnO increase the density of concrete, minimizing the pores in the concrete and consequently increasing the strength of concrete. The solutions are simplified to the corresponding solutions of the integer ordered model of Jeffrey-nanofluid. Applications of this work can be found in construction engineering and management such as buildings, roads, tunnels, bridges, airports, railroads, dams, and utilities.

Keywords: concrete; Jeffrey nanofluid; Z_nO nanoparticles; channel flow; Atangana–Baleanue fractional derivative

1. Introduction

One of the recent areas of research is nanotechnology, which covers a wide range of studies in civil engineering and construction. To control the hydration, development of resistance, corrosion, and fracture in the cement-based material, it is important to have good knowledge of the nanostructure of cement-based materials. For many construction circumstances, the improvement of materials with new characteristics, such as self-cleaning, fade resistance, high anti-gravity, and scratch protection and wear resistance, is very important [1–3]. Recently, nano-research in cement has concentrated on investigating the composition of cement-based materials and their fracture mechanisms [4–8]. There are several experimental reports on incorporating nanoparticles in cement-based concrete. Hadi et al. [9], analyzed Al_2O_3 nanoparticles concentration and environmental effect on the cogeneration system in the cement industry. The results showed that the compressive strength of the cement is improved compared to the plane cement when checked at the seventh and twenty-eighth day. Nazari et al. [10], investigated the effect of Al_2O_3 nanoparticles on the compressive strength and workability of blended concrete.

Their analysis revealed that the strength of the cement is increased by adding the nanoparticles at the rate of up to 2.0%. The interesting part of the analysis is that the ultimate strength is gained by dispersing 1.0% of nanoparticles. Morsey et al. [11] studied the experimentally hybrid effect of carbon nanotubes (CNTs) and nano clay on the physicomechanical properties of cement mortar and also show the compressive strength, phase composition, and microstructure of blended cement. Malothra and Mehta [12] analyzed the high-volume fly ash technology in which fly ash replaces more than half of the portland cement in concrete. The study covers the applications of concrete in sustainable development, fly ash characteristics, mechanisms by which fly ash improves the characteristics of concrete, the definition of high-performance high volumes fly ash (HVFA) concrete and history of its development, concrete mixture proportions, properties of fresh and hardened concrete, the durability of high-performance HVFA concrete, HVFA concrete construction practice, and case histories describing the use of HVFA concrete in Canada and the United States. Raki et al. [13], researched in the area of concrete, using the nanoparticles and nanotubes to improve the quality of the concrete. They have concluded that when nano-$CaCO_3$ has added to the cement the rate of heat development enhanced rapidly. In a research article, Bahamani et al. [14] stated that when SiO_2 nanoparticles are added to cement-treated soil for stabilization, the compressive strength is improved by 80%. Shekari and Razzaghi [15], investigated the durability and strengths of concrete in their analysis. The results are interesting and important because, both the mechanical properties and durability are checked, and they concluded that these properties are improved by adding nanoparticles in concrete. Moreover, the aluminum nanoparticles are the most effective one amongst all the tested nanoparticles in this study. The influence of the size of silicon oxide nanoparticles on the double blended concrete was analyzed by Givi et al. [16] through an experiment. The results showed that the concrete with small size of nanoparticles (15 nm) was harder than the concrete with large size of nanoparticles (80 nm). Many scholars have studied the mechanical properties of cement mortars, including nano-Fe_2O_3 and nano- SiO_2 [17–21]. In other sectors the applications of nanofluids are also studied by various researchers. Goodarzi et al. [22] investigated the two phase flow of nanofluid in a shallow cavity. Arasteh et al. [23] have used the nanofluids to enhance the working capacity of double-layered heat. Yousefzadeh et al. [24] have presented a numerical modelling and investigation for the flow of nanofluid with different heat transfer areas. They have used the solid silver nanoparticles having volume fraction 0%, 2%, and 4% in the base fluids to enhance the heat transfer. Ahmadi et al. [25] have used various machine learning methods including MPR (Multivariable Polynomial Regression), MARS (Multivariate Adaptive Regression Splines), ANN-MLP (Artificial Neural Network- Multilayer Perceptron), and GMDH (Group Method of Data Handling), for modeling the dynamic viscosity of CuO/water nanofluid based on the temperature, concentration, and size of nanostructures. They have concluded that the concentration of the nanoparticles has the highest importance, while the size has least importance. The heat transfer in pseudo-plastic non-Newtonian nanofluid with suction and injection was studied by Maleki et al. [26]. They have claimed that in the case of injection the heat transfer reduces in non-Newtonian nanofluids. Safaei et al. [27] numerically studied flow of nanofluid with carbon nanotubes over a forward-facing step. Their results show that heat transfer is remarkably affected by the volume fraction and Reynolds number. Gholamalizadeh et al. [28] studied the effects of forced convection on the flow of nanofluids and have mentioned that porosity does not bring any change in the velocity of nanofluid in this case. Jalali et al. [29] investigated the flow of oil based nanofluid with MWCNTs (Multiwall Carbon Nanotubes) nanoparticles. Other related studies can be found in [30–35] and the references therein.

Zinc oxide has unique physical and chemical properties, due to this reason it may be called a material with various functions. Zinc oxide with its specific properties, such as high electrochemical coupling-coefficient, chemical stability, high photo-stability, rigidity, hardness, a piezoelectric constant, and a huge range of radiation, is a material with several functions. It is an essential material in the ceramic industry, while its toxic behavior, bio-degradability, and bio-compatibility make it a material of interest for bio-medicine and pre-ecological system [36–38]. Due to its varied characteristics,

both physical and chemical, zinc oxide is used in many areas, like, bioengineering, cement industry, tires, ceramics, pharmaceuticals, agriculture, and paints. Apart from these applications mentioned above, zinc oxide can be used in other branches of industry, like concrete production. The processing time, speed of hydration reaction, compressive strength, slowdown hardening, and quenching can be improved by the dispersion of zinc oxide. Nochaiya et al. [39] experimentally analyzed the effect of ZnO nanoparticles on cement hydration, they have noted a decrease in setting time and porosity of mortars cement and also an increase in the compressive strength of concrete was found. The mechanical properties of self-compacting concrete were investigated after the addition of a different amount of ZnO nanoparticles by Arefi and Rezaei-Zarchi [40]. Flores-Velez et al. [41] studied the properties and characterization of portland cement composite incorporating zinc iron oxide. The $ZnFe_2O_4$ nanoparticles have been taken, in their research, to analyze the compressive strength of the cement paste. This research article revealed that the strength of is attained after 42 days. After that Taylor-Lenge et al. [42], studied to improve the reactivity of metakaolin cement blends using zinc oxide. They have mentioned that ZnO nanoparticles behave like a delayed accelerator for cement slurry. To improve the biological and mechanical properties of dental cement, Nguyen et al. [43] considered the ZnO nanoparticles. They have mentioned that besides the anti-bacterial characteristics of ZnO nanoparticles also significantly, enhanced the compressive strength and tensile strength of the cement. Gowda et al. [44], studied the influence of nano-zinc and nano-silica on the compressive strength of the mortar cement. Their results show that the strength of the cement is improved when nano-zinc and nano-silica are dispersed in the cement slurry.

Fractional calculus has been growing nowadays, vastly, due to its versatile and unique properties. The non-integer order derivative is solved through fractional calculus tools. Fractional calculus is the extension of classical calculus and it has been for approximately three centuries. Fractional calculus is an important and fruitful tool for describing many systems including memory. In the last few years, fractional calculus is used for many purposes in various fields, such as electrochemistry, transportation of water in ground level, electromagnetism, elasticity, diffusion, and in conduction of heat process. In 2016, Atangana and Baleanu [45], developed a modern definition with a generalized exponential function, namely, the Mittag Leffler function. The kernel of the integral associated with this derivative is non-local and non-singular. Atangana and Koca [46], used the new definition of the fractional derivative to a simple non-linear system to show the existence and uniqueness of the solution for the system. After that several researchers used the Atangana–Baleanu fractional derivative in their work. Ali et al. [47] studied Casson fluid using the fractional derivative approach. Their research was on the non-Newtonian behavior of blood flow in a cylinder. Using the idea of fractional derivatives, Khan et al. [48] studied the flow of nanofluids, in which sodium alginate is chosen is a base fluid. They have generalized the model with Atangana–Baleanu (AB) derivative. Sheikh et al. [49,50] have used the idea of Atangana–Baleanu fractional derivatives for the flow problem of Casson fluid and exact solutions are obtained. They have presented the comparison of the two newly developed fractional operators, namely, Atangana–Baleanu and Caputo–Fabrizio fractional derivatives in their articles. They have concluded in both articles that the velocity profile obtained for the fractional model with Atangana–Baleanu derivatives comes to steady-state more rapidly compared to the velocity profile for CF (Caputo Fabrizio) derivatives. The problem related to nanofluids is modeled using the AB fractional derivatives by Sheikh et al. [51]. The authors have used the fractional derivatives approach to model the nanofluid flow and its applications in solar energy is explained. The analysis reveals the efficiency of the solar collector is enhanced by adding nanoparticles to the working fluid. Using the concept of fractional derivatives, Asif et al. [52] studied the fluid flow between two parallel plates. They have also considered the arbitrary shear stress on the boundary. Gohar et al. [53], presented the study of hybrid nanofluids using the fractional derivatives and discussed their application in the cement-based materials. Atangana and Koca [46], extended the idea of Atangana and Baleanu and applied the derivative to a simple nonlinear system. The analysis shows that the solution for the fractional derivatives exists and is unique. In another article, Atangana and Koca [54] claimed that they have

refined the existing derivative with a more generalized Mittage–Leffler function called the Prabhakar function. They have presented some new and interesting results. The efficiency of solar collectors was studied by Sheikh et al. [55] in another paper using the Atangana–Baleanu fractional derivatives approach. They have considered the inclined plate in their study to have a better understanding of the solar collectors. They have concluded that the performance of the solar collectors may be improved by adding the cerium oxide nanoparticles. Vieru et al. [56] studied the flow of viscoelastic fluid using fractional derivative approach. The flow was considered between two side walls perpendicular to the plate. The solutions were found using the Fourier and Laplace transforms. Siddique and Vieru [57] discussed the flow of Newtonian fluid under the slip condition at the boundary. The model was generalized using the concept of time fractional derivatives. Other studies on AB fractional derivative can be found in [54,58,59].

In everyday life, non-Newtonian fluids, like lava, gums, and blood, are widely used in different fields of industries such as food industries, biomedicine, and chemical engineering, which make it necessary for us to study non-Newtonian fluid flow behavior. Non-Newtonian fluid attributes incorporate shear diminishing, viscoelasticity [60], viscoplasticity [61], and shear thickening conduct. Due to its complex behavior, various models in the literature are suggested for non-Newtonian fluids, one of them is Jeffrey fluid model with relaxation and retardation time. From the detailed survey of the published literature it is revealed that so far, no study is carried out to study the Jeffrey nanofluid flow with heat transfer and mass concentration in a channel. Moreover, these studies are even rare for other simple fluid models with fractional derivatives. In the present article, we have taken the convective flow of Jeffrey nanofluid in the channel. The model is fractionalized using the fractional derivative approach proposed by Atangana and Baleanu [45]. The fractional PDEs are solved by applying the Laplace transform technique. Furthermore, the solutions are plotted, and the results are discussed with applications in the cement-based materials.

2. Mathematical Modelling

The flow of Jeffrey nanofluid is considered in a channel with heat transfer and mass concentration. d is the distance between the walls of the channel. The flow of the fluid is taken along the x-direction while the y-axis is chosen normal to the flow of the fluid. Initially, the fluid is considered stationary with ambient temperature and mass concentration. Initially, the temperature raised to the wall temperature and the concentration to the wall concentration which boost up the buoyancy forces. The plate at $y = d$ is oscillating with the cosine oscillations as shown in Figure 1.

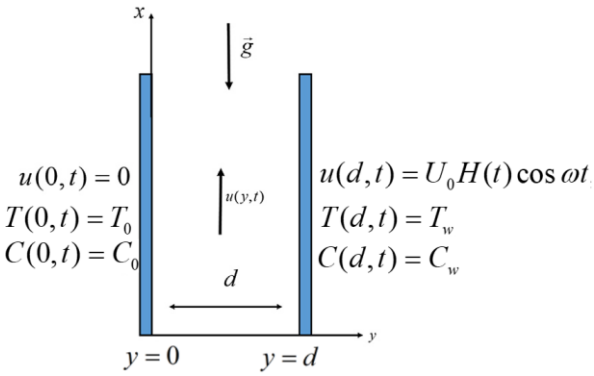

Figure 1. Geometry of the flow.

The constitutive equations of the defined flow system are given as under [62].

$$\rho_{nf}\frac{\partial u(y,t)}{\partial t} = \mu_{nf}\left(1 + \lambda_2\frac{\partial}{\partial t}\right)\frac{\partial^2 u(y,t)}{\partial y^2} - \sigma_{nf}{B_0}^2 u(y,t) + (\rho\beta_T)_{nf} g(T - T_0) + (\rho\beta_C)_{nf} g(C - C_0), \quad (1)$$

The heat transfer and mass concentration are considered in the flow regime. The energy and mass equation are derived and are presented in their final form as [63]:

$$\left(\rho c_p\right)_{nf}\frac{\partial T(y,t)}{\partial t} = k_{nf}\frac{\partial^2 T(y,t)}{\partial y^2}, \tag{2}$$

$$\frac{\partial C(y,t)}{\partial t} = D_{nf}\frac{\partial^2 C(y,t)}{\partial y^2}, \tag{3}$$

The corresponding initial constraints are given as:

$$u(y,\,0) = 0,\; T(y,\,0) = T_0,\; C(y,0) = C_0, \tag{4}$$

As the flow is considered in the channel and the distance between the wall is denoted by d, the boundary conditions are given in the following form (Equation (5)). On the plate at $y = 0$, there is no motion of the fluid and the temperature and concentration are considered as ambient, while at $y = d$ the oscillations of the plate are considered and temperature and concentrations raised to T_w and C_w, respectively.

$$\left.\begin{array}{c} u(0,\,t) = 0,\; T(0,\,t) = T_0,\; C(0,t) = C_0 \\ u(d,\,t) = U_0 H(t)\cos\omega t,\; T(d,\,t) = T_w,\; C(d,t) = C_w \end{array}\right\}. \tag{5}$$

For nanofluids, the expressions of μ_{nf}, $(\rho\beta_T)_{nf}$, and $(\rho c_p)_{nf}$ are given by [64].
Using the Buckingham pi theorem, the following dimensionless variables are introduced:

$$v = \frac{u}{U_0}, \xi = \frac{y}{d}, \tau = \frac{U_0}{d}t, \Theta = \frac{T-T_0}{T_w-T_0}, \Phi = \frac{C-C_0}{C_w-C_0},$$

Using these variables into Equations (1)–(5), we get, (dropped * sign for convenience)

$$\frac{\partial v}{\partial \tau} = \phi_7\frac{\partial^2 v}{\partial \xi^2} + \phi_7\lambda\frac{\partial^3 v}{\partial \tau \partial \xi^2} - \phi_8 M v + \phi_9 Gr\Theta + \phi_{10} Gm\Phi\,, \tag{6}$$

$$\frac{\partial \Theta}{\partial \tau} = \frac{1}{a_0}\frac{\partial^2 \Theta}{\partial \xi^2}, \tag{7}$$

$$\frac{\partial \Phi}{\partial \tau} = \frac{1}{a_1}\frac{\partial^2 \Phi}{\partial \xi^2}, \tag{8}$$

Also, the initial and boundary constraints are nondimensionalized and are given as:

$$\left.\begin{array}{ll} v(\xi,\,0) = 0, & \Theta(\xi,\,0) = 0, \\ v(0,\,\tau) = 0, & \Theta(0,\,\tau) = 0, \\ v(1,\,\tau) = H(\tau)\cos\omega\tau, & \Theta(1,\,\tau) = 1, \end{array}\right\}, \tag{9}$$

The following constants and dimensionless parameters appear during the process of nondimensionalization:

$$\phi_1 = (1-\phi) + \phi\left(\frac{\rho_s}{\rho_f}\right),\; \phi_2 = 1 + 3\frac{(\sigma-1)\phi}{(\sigma+2)-(\sigma-1)\phi},\; \phi_3 = (1-\phi) + \phi\left(\frac{\rho_s\beta_{Ts}}{\rho_f\beta_f}\right),$$
$$\phi_4 = (1-\phi) + \phi\left(\frac{\rho_s\beta_{Cs}}{\rho_f\beta_f}\right),\; \phi_5 = \frac{1}{(1-\phi)^{2.5}},\; \phi_6 = \frac{\phi_5}{\phi_1 \mathrm{R_a}},\; \phi_7 = \frac{\phi_6}{1+\lambda_1},\; \phi_8 = \frac{\phi_2}{\phi_1},\; \phi_9 = \frac{\phi_3}{\phi_1},$$
$$\phi_{10} = \frac{\phi_4}{\phi_1},\; \phi_{11} = (1-\phi) + \phi\frac{\rho_s c_{ps}}{\rho_f c_{pf}},\; a_0 = \frac{Pe\phi_{11}}{\lambda_f},\; a_1 = \frac{Sc}{(1-\phi)},\; \lambda_f = \frac{k_{nf}}{k_f}.$$

3. Generalization of the Classical Model

Replacing $\frac{\partial(.)}{\partial\tau}$ by AB fractional derivative, Equations (6)–(8) can be written as:

$$\wp_t^\alpha v = \phi_7 \frac{\partial^2 v}{\partial \xi^2} + \phi_7 \lambda \wp_t^\alpha (\frac{\partial^2 v}{\partial \xi^2}) - \mathfrak{R}_0 v + \mathfrak{R}_1 \Theta + \mathfrak{R}_2 \Phi. \tag{10}$$

$$\wp_t^\alpha \Theta = \frac{1}{a_0} \frac{\partial^2 \Theta}{\partial \xi^2}, \tag{11}$$

$$\wp_t^\alpha \Phi = \frac{1}{a_1} \frac{\partial^2 \Phi}{\partial \xi^2}, \tag{12}$$

where

$$\mathfrak{R}_0 = \mathrm{M}\phi_8, \;\; \mathfrak{R}_1 = Gr\phi_9, \;\; \mathfrak{R}_2 = Gm\phi_{10},$$

The proposed model by Atangana and Baleanu [45,46,50] for fractional derivatives based on the generalized exponential function is given by:

$$\wp_\tau^\delta s(\tau) = \frac{\aleph(\delta)}{1-\delta} \int_0^\tau E_\delta \left(\frac{-\delta(\tau - t)^\delta}{1-\delta} \right) s'(\tau) dt, \text{ for } 0 < \delta < 1, \; \aleph(1) = \aleph(0) = 1. \tag{13}$$

Here, $E_\delta(-t^\delta) = \sum_{\vartheta=0}^{\infty} \frac{(-t)^{\delta k}}{\Gamma(\delta\vartheta+1)}$, is the Mittag–Leffler function [51].

4. The Solution of the Heat and Mass Equations

Applying fractional Laplace transformation on Equations (11) and (12) using Equation (13) and boundary conditions from Equation (9) yield to the following:

$$\frac{d^2\overline{\Theta}(\xi,\, q)}{d\xi^2} - \frac{b_2 q^\alpha}{q^\alpha + b_1} \overline{\Theta}(\xi,\, q) = 0, \tag{14}$$

$$\overline{\Theta}(0,\, q) = 0, \; \overline{\Theta}(1,\, q) = \frac{1}{q}, \tag{15}$$

$$\frac{d^2\overline{\Phi}(\xi,\, q)}{d\xi^2} - \frac{b_3 q^\alpha}{q^\alpha + b_1} \overline{\Phi}(\xi,\, q) = 0, \tag{16}$$

$$\overline{\Phi}(0,\, q) = 0, \; \overline{\Phi}(1,\, q) = \frac{1}{q}, \tag{17}$$

where

$$b_0 = \frac{1}{1-\alpha}, \;\; b_1 = \alpha b_0, \;\; b_2 = a_0 b_0, \;\; b_3 = a_1 b_0.$$

The solution of energy and concentration equations i.e., Equations (14) and (16), respectively, using the transformed boundary conditions, Equations (15) and (17) is given by:

$$\overline{\Theta}(\xi,\, q) = \frac{1}{q} \frac{\sinh\xi \sqrt{\frac{b_2 q^\alpha}{q^\alpha + b_1}}}{\sinh \sqrt{\frac{b_2 q^\alpha}{q^\alpha + b_1}}}, \tag{18}$$

$$\overline{\Phi}(\xi,\, q) = \frac{1}{q} \frac{\sinh\xi \sqrt{\frac{b_3 q^\alpha}{q^\alpha + b_1}}}{\sinh \sqrt{\frac{b_3 q^\alpha}{q^\alpha + b_1}}}, \tag{19}$$

Equations (18) and (19) present the solutions of Equations (14) and (16) in the transformed variable q. To obtain the inverse Laplace transform by using the inversion method by Zakian [65], we get

$$\theta(\xi,\ t) = \frac{2}{t}\sum_{j=1}^{N} \mathrm{Re}\Big\{K_j \overline{\theta}(\xi, \frac{\alpha_j}{t})\Big\}, \tag{20}$$

$$\Phi(\xi,\ t) = \frac{2}{t}\sum_{j=1}^{N} \mathrm{Re}\Big\{K_j \overline{\Phi}(\xi, \frac{\alpha_j}{t})\Big\}, \tag{21}$$

where K_j and α_j are given in Table 1.

Table 1. The values of involved terms in the Zakian method for Laplace inverse [65].

j	K_j	α_j
1	$12.83767675 + i\ 1.666063445$	$-36902.0821 + i\ 196990.4257$
2	$12.22613209 + i\ 5.012718792$	$61277.02524\ - i\ 95408.62551$
3	$10.93430308 + i\ 8.409673116$	$-28916.56288 + i\ 18169.18531$
4	$8.776434715 + i\ 11.92185389$	$4655.361138\ - i\ 1.901528642$
5	$5.225453361 + i\ 15.72952905$	$-118.7414011\ - i\ 141.3036911$

5. Velocity Profile Calculations

To find the solution of the momentum equation, keeping into consideration Equation (13), the Laplace transformation of Equation (10) and the imposed boundary conditions (9) is presented as follow:

$$\begin{aligned} &\tfrac{d^2\overline{v}(\xi,\ q)}{d\xi^2} - \tfrac{b_4 q^\alpha}{b_6 q^\alpha + b_1}\overline{v}(\xi,\ q) - \mathfrak{R}_3\Big[\tfrac{q^\alpha + b_1}{b_6 q^\alpha + b_1}\Big]\overline{v}(\xi,\ q) \\ &= -\mathfrak{R}_4\Big[\tfrac{q^\alpha + b_1}{b_6 q^\alpha + b_1}\Big]\overline{\Theta}(\xi,\ q) - \mathfrak{R}_5\Big[\tfrac{q^\alpha + b_1}{b_6 q^\alpha + b_1}\Big]\overline{\Phi}(\xi,\ q), \end{aligned} \tag{22}$$

For

$$\overline{v}(0,\ q) = 0,\ \overline{v}(1,\ q) = \frac{q}{q^2 + \omega^2}. \tag{23}$$

Solving the differential equation, Equation (22), using Equation (23) the solution is transformed form is given as under.

$$\begin{aligned} \overline{v}(\xi, q) = &\left[\frac{q}{q^2+\omega^2}\frac{\sinh\xi\sqrt{\frac{b_{11}(q^\alpha+b_9)}{q^\alpha+b_{10}}}}{\sinh\sqrt{\frac{b_{11}(q^\alpha+b_9)}{q^\alpha+b_{10}}}}\right] + \left[\frac{\mathfrak{R}_4(q^\alpha+b_1)(q^\alpha+b_1)}{q\begin{pmatrix} b_2 q^\alpha(b_6 q^\alpha + b_1) \\ -(b_7 q^\alpha + b_8)(q^\alpha + b_1)\end{pmatrix}}\right]\left[\frac{\sinh\xi\sqrt{\frac{b_{11}(q^\alpha+b_9)}{q^\alpha+b_{10}}}}{\sinh\sqrt{\frac{b_{11}(q^\alpha+b_9)}{q^\alpha+b_{10}}}} - \frac{\sinh\xi\sqrt{\frac{b_2 q^\alpha}{q^\alpha+b_1}}}{\sinh\sqrt{\frac{b_2 q^\alpha}{q^\alpha+b_1}}}\right] \\ &+\left[\frac{\mathfrak{R}_5(q^\alpha+b_1)(q^\alpha+b_1)}{q\begin{pmatrix} b_3 q^\alpha(b_6 q^\alpha + b_1) \\ -(b_7 q^\alpha + b_8)(q^\alpha + b_1)\end{pmatrix}}\right]\left[\frac{\sinh\xi\sqrt{\frac{b_{11}(q^\alpha+b_9)}{q^\alpha+b_{10}}}}{\sinh\sqrt{\frac{b_{11}(q^\alpha+b_9)}{q^\alpha+b_{10}}}} - \frac{\sinh\xi\sqrt{\frac{b_3 q^\alpha}{q^\alpha+b_1}}}{\sinh\sqrt{\frac{b_3 q^\alpha}{q^\alpha+b_1}}}\right]. \end{aligned} \tag{24}$$

where

$$b_4 = \frac{b_0}{\phi_7},\ b_5 = b_0\lambda,\ \mathfrak{R}_3 = \frac{\mathfrak{R}_0}{\phi_7},\ \mathfrak{R}_4 = \frac{\mathfrak{R}_1}{\phi_7},\ \mathfrak{R}_5 = \frac{\mathfrak{R}_2}{\phi_7}\ .$$

Taking the inverse Laplace transform of Equation (24), by using the inversion method by Zakian [65], we get:

$$v(\xi,\ t) = \frac{2}{t}\sum_{j=1}^{N} \mathrm{Re}\Big\{K_j \overline{v}(\xi, \frac{\alpha_j}{t})\Big\}, \tag{25}$$

where K_j and α_j are given in Table 1.

6. Skin Friction, Rate of Heat Transfer, and Rate of Mass Transfer

Friction between the fluid and the solid boundary is termed as skin friction. This is an important physical quantity for engineers and experimenters. The expression for non-dimensional skin friction is given as:

$$C_f = \left(\frac{1}{1+\lambda_1}\right)(1+\lambda D_t{}^{\alpha})\frac{\partial v}{\partial \xi}(\xi,\tau)\bigg|_{\xi=0}, \tag{26}$$

The ratio of convective energy to the fluid to conductive energy from the fluid is defined as rate of heat transfer (Nusselt number), the name is set after a German mathematician Wilhelm Nusselt. The non-dimensional Nusselt number is given by:

$$\mathrm{Nu} = -\lambda_{nf}\frac{\partial \Theta}{\partial \xi}\bigg|_{\xi=0}, \tag{27}$$

From the concentration profile, an important physical quantity, rate of mass transfer (Sherwood number) is calculated and in dimensionless form is given as:

$$S_h = D_{nf}\frac{\partial \Phi}{\partial \tau}(\xi,\tau)\bigg|_{\xi=0}. \tag{28}$$

7. Parametric Study

The channel flow of viscoelastic Jeffrey nanofluid with suspended zinc-oxide nanoparticles over an oscillating, vertical plate is considered in this analysis. The modern concept of the non-integer order derivative is utilized to generalize the model. The coupled fractional PDEs with AB time-fractional derivatives are solved by an integral transformation called Laplace transform technique. The numerical values of thermo-physical properties of zinc-oxide and concrete, which is chosen as the base fluid, are mentioned in Table 2. Table 3 shows the variation in skin friction for different values of volume fraction, which shows that by increasing volume fraction ϕ, from range (0.01–0.04) skin friction enhanced from 8.22–15.26%, which may enhance the mechanical strength of concrete, by comparing present results to Gohar et al. [53], it is observed that by adding Al_2O_3, skin friction enhance up to 10.73% and the skin friction increases up to 10.75% by adding *MWCNT's*. However, from the present study we notice that skin friction enhances up to 15.26% by adding *ZnO* nanoparticles, this means that *ZnO* are more effective to strengthen the concrete. Table 4 shows the variation in Nusselt number for different values of volume fraction, which shows that the heat transfer rate is increased by increasing volume fraction.

Table 2. Thermo-physical properties of nanoparticles and base fluid.

Properties	Concrete	*ZnO*
$\rho(\mathrm{kgm}^{-3})$	2300	5.61×10^{3}
$k(\mathrm{Wm}^{-1}\mathrm{K}^{-1})$	1.160	1.046
$C_p(\mathrm{kg}^{-1}\mathrm{K}^{-1})$	41.086	0.880
$\beta\times10^{-5}(\mathrm{K}^{-1})$	1.57	1.25

Table 3. Variations in shear stress on the boundary for different values of ϕ.

ϕ	α	λ	λ_1	τ	C_f	Enhancement (%)
0.00	0.2	0.5	0.5	2	0.596	
0.01	0.2	0.5	0.5	2	0.645	8.221%
0.02	0.2	0.5	0.5	2	0.669	12.24%
0.03	0.2	0.5	0.5	2	0.681	14.26%
0.04	0.2	0.5	0.5	2	0.687	15.26%

Table 4. Variations in Nusselt Number for different values of ϕ.

ϕ	τ	α	Nu	Enhancement (%)
0.00	2	0.2	0.603	
0.01	2	0.2	0.675	11.94%
0.02	2	0.2	0.758	25.70%
0.03	2	0.2	0.854	41.62%
0.04	2	0.2	0.969	60.69%

Figures 2–5, are sketched to display the influence of volume fraction on different profiles i.e., velocity, temperature, Nusselt number, and skin friction. In Figure 2, we can see that the velocity decreases upon increasing the values of volume fraction, and it is observed from the figure that nanofluid is denser as compared to the ordinary fluid. Keeping in view the applications of *ZnO*-nanoparticles in concrete, from this figure it is noticed that by suspending *ZnO*-nanoparticles the concrete will be denser and hence it will gain strength. Enhancement in volume fraction also increases density, reduces porosity by decreasing air content in concrete, and improves the bond between the cement matrix and aggregates. Due to these properties, cohesiveness of concrete increases reducing workability, permeability of water through *ZnO* incorporated concrete decreases, and mechanical strength increases [66].

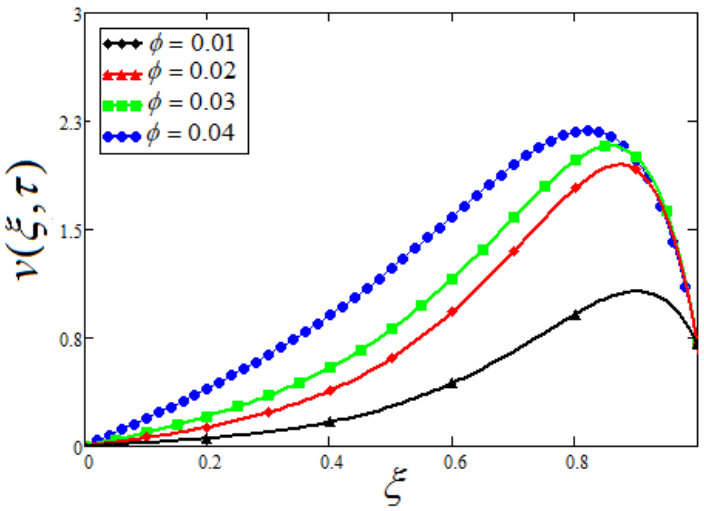

Figure 2. Variation in velocity profile for different values of ϕ when $Gr = 5, \alpha = 0.2, \mathrm{P}e = 0.2, M = 0.3, \tau = 1,\ \lambda = 1.5, \lambda_1 = 0.5$.

Figure 3 is plotted to exhibit variation in volume fraction for temperature profile, it is clear from the figure that temperature increases due to increase in volume fraction, the physics behind this is that the thermal conductivity of Jeffrey nanofluid increases by increasing volume fraction, which enhances the boundary layer thickness and hence temperature increases. Figure 4 is sketched for very important phenomena Nusselt number against volume fraction, it is observed from the figure that heat transfer rate increases due to the increase in volume fraction. Figure 5 is plotted to show the effect of volume fraction on skin friction and depict the same behavior as discussed in Table 3. This figure reveals that by increasing volume fraction ϕ, from range (0.01–0.04), the skin friction enhances which may enhance the mechanical strength of concrete, by comparing present results to Gohar et al. [53], it is observed that by adding Al_2O_3, skin friction enhances up to 10.73% and the skin friction increases up to 10.75% by adding *MWCNT's*. However, from the present study we notice that skin friction enhances up to 15.26% by adding *ZnO* nanoparticles, this means that *ZnO* are more effective to strengthen the concrete.

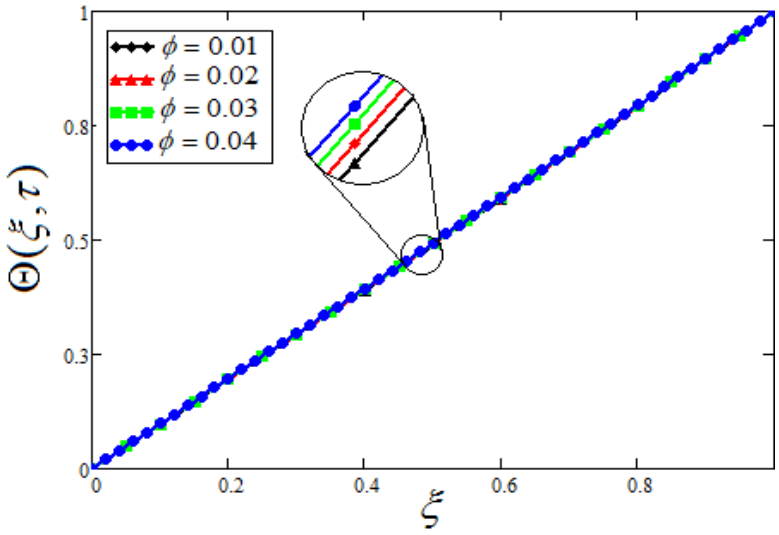

Figure 3. Variation in temperature profile for different values of ϕ when $Gr = 5, \alpha = 0.2, \mathrm{P}e = 0.2, M = 0.3, \tau = 1,\ \lambda = 1.5, \lambda_1 = 0.5$.

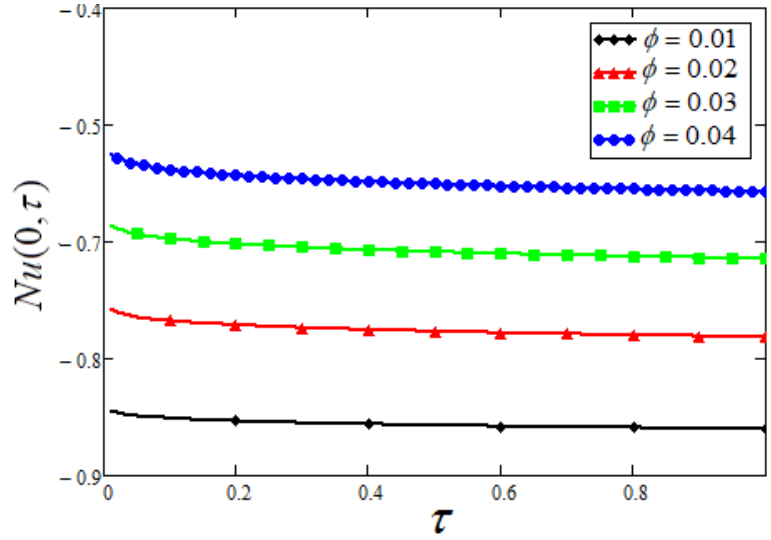

Figure 4. Variation in Nusselt number for different values of ϕ when $Gr = 5, \alpha = 0.2, \mathrm{P}e = 0.2, M = 0.3, \tau = 1,\ \lambda = 1.5, \lambda_1 = 0.5$.

Graphical results for fractional parameter on both velocity and temperature profiles are displayed in Figures 6 and 7, both figures show the same behavior. By increasing the fractional parameter α, there are different plots. This means that we can calculate the velocity or temperature for any value of the fractional parameter, which is termed as the memory effect. Hence the fractional parameter is, in fact, the memory parameter. Figures 8 and 9 are drawn to show the effect of λ_1 and λ on velocity profile, it is observed that both the graphs show the opposite behavior. From Figure 8, it is observed that the velocity of Jeffrey nanofluid is increased by increasing λ_1, this physically means that increasing values of relaxation time parameter λ_1, actually decreases the viscoelasticity of nanofluid. However, the opposite trend is noticed in Figure 9, which shows the effect of Jeffrey fluid parameter λ on fluid velocity. Physically, λ increases viscous forces or increasing the non-Newtonian behavior and as a result, the thickness of the boundary layer enhances, that is why the fluid velocity decreases.

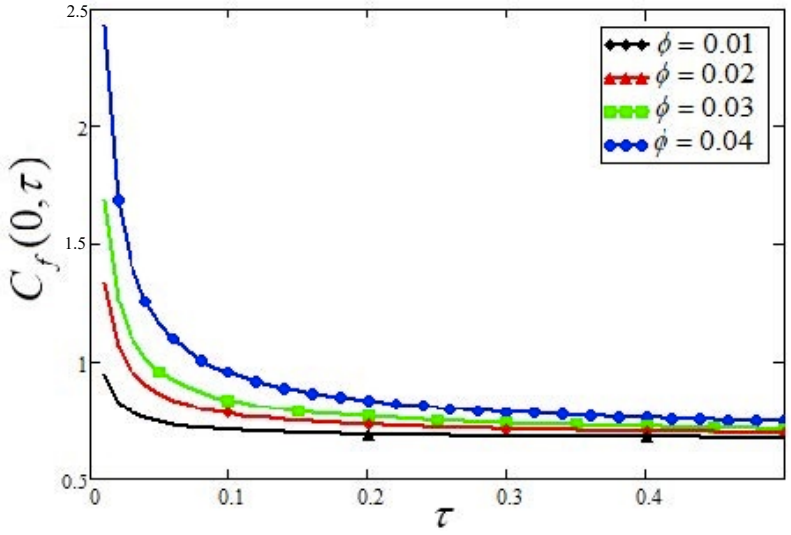

Figure 5. Variation in skin friction for different values of ϕ when $Gr = 5, \alpha = 0.2, \mathrm{P}e = 0.2, M = 0.3, \tau = 1,\ \lambda = 1.5, \lambda_1 = 0.5$.

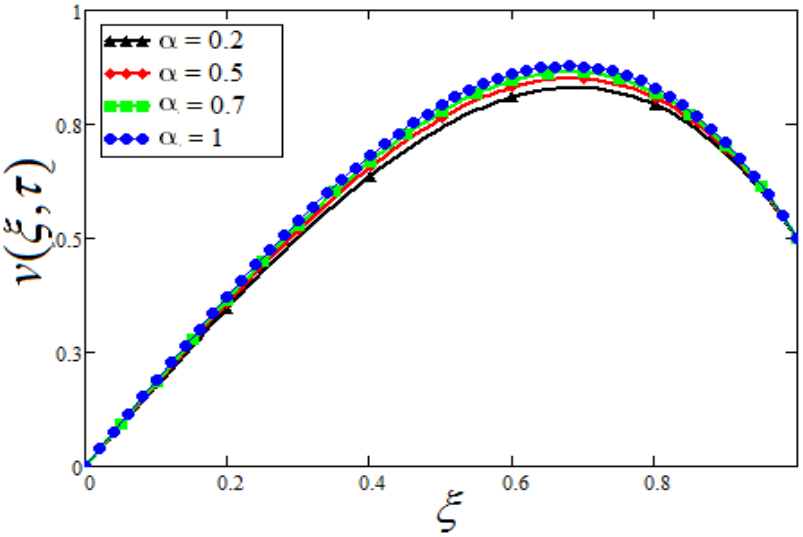

Figure 6. Variation in velocity profile for different values of α when $Gr = 5, \phi = 0.02, \mathrm{P}e = 0.2, M = 0.3, \tau = 1,\ \lambda = 1.5, \lambda_1 = 0.5$.

Figure 10 depicts the variation in velocity profile for different values of *Gr*. It is clear from the figure that velocity is higher for greater values of *Gr* and is minimum for smaller values of *Gr*. Physically, lower values of *Gr* means higher viscosity. In the present study, we are discussing cementitious materials, in which lower values of Gr will be helpful. Figure 11 is drawn for different values of mass Grashof number *Gm* which shows for a large value of *Gm*, the buoyancy forces increases and consequently accelerate the flow, and the opposite behavior is noticed in Figure 12 which is sketched for the magnetic parameter *M*. The electrically conducting fluid is exposed to a magnetic field which produces Lorentz's forces in the fluid. These forces are flow opposing forces and as a result, retards the velocity of the fluid.

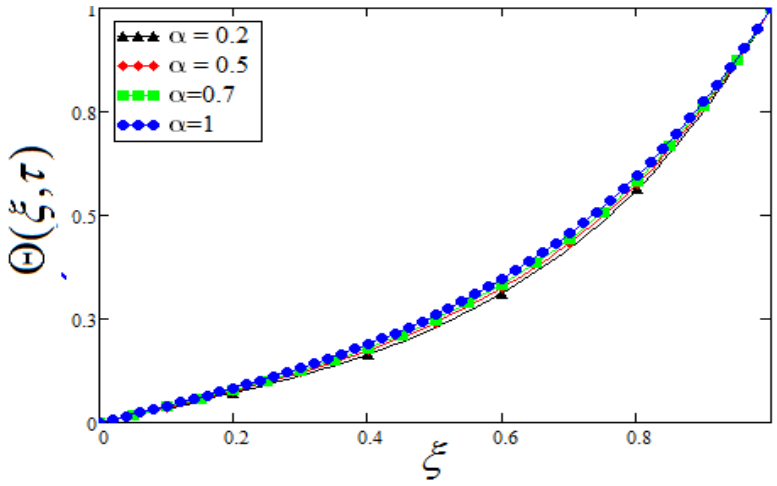

Figure 7. Variation in temperature profile for different values of α when $Gr = 5, \phi = 0.02, \mathrm{P}e = 0.2, M = 0.3, \tau = 1,\ \lambda = 1.5, \lambda_1 = 0.5$.

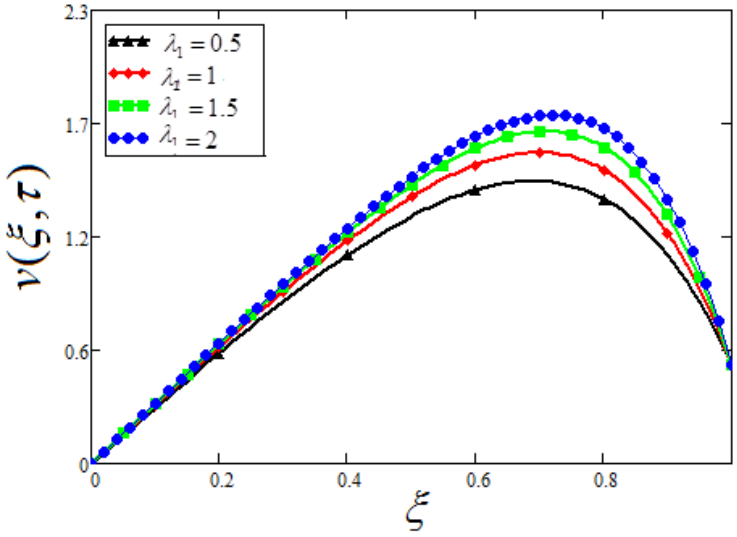

Figure 8. Variation in velocity profile for different values of λ_1 when $Gr = 5, \alpha = 0.2, \mathrm{P}e = 0.2, M = 0.3, \tau = 1,\ \phi = 0.02, \lambda = 1.5$.

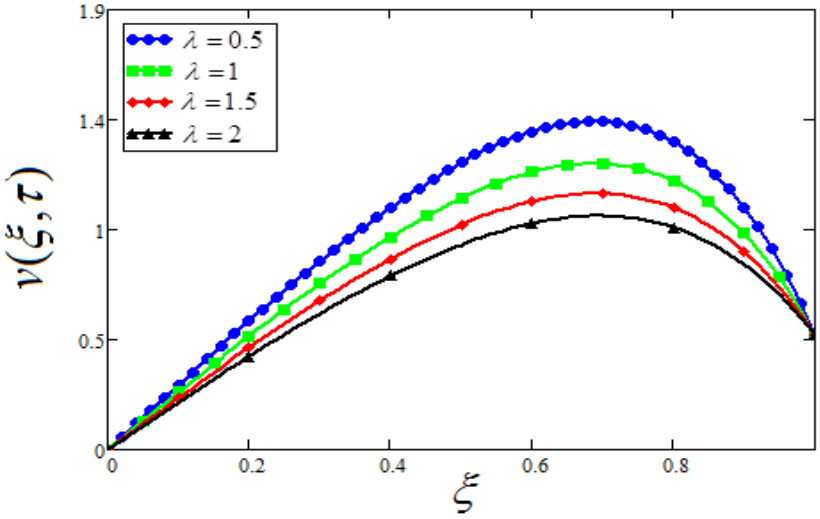

Figure 9. Variation in velocity profile for different values of λ when $Gr = 5, \alpha = 0.2, \mathrm{P}e = 0.2, M = 0.3, \tau = 1,\ \phi = 0.02, \lambda_1 = 0.5$.

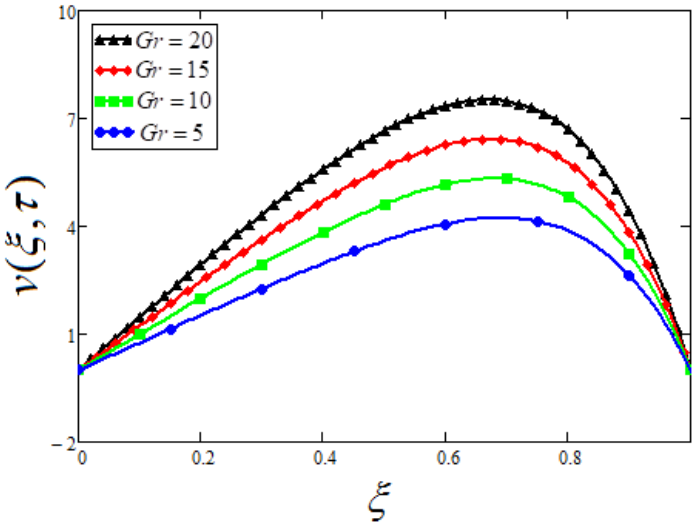

Figure 10. Variation in velocity profile for different values of Gr when $\lambda_1 = 0.5, \alpha = 0.2, \mathrm{P}e = 0.2, M = 0.3, \tau = 1,\ \phi = 0.02, \lambda = 1.5$.

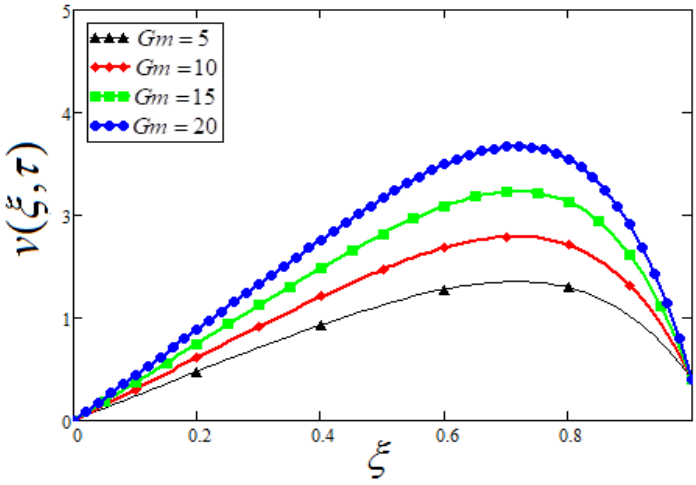

Figure 11. Variation in velocity profile for different values of Gm when $\lambda_1 = 0.5, \alpha = 0.2, \mathrm{P}e = 0.2, M = 0.3, \tau = 1,\ \phi = 0.02, \lambda = 1.5$.

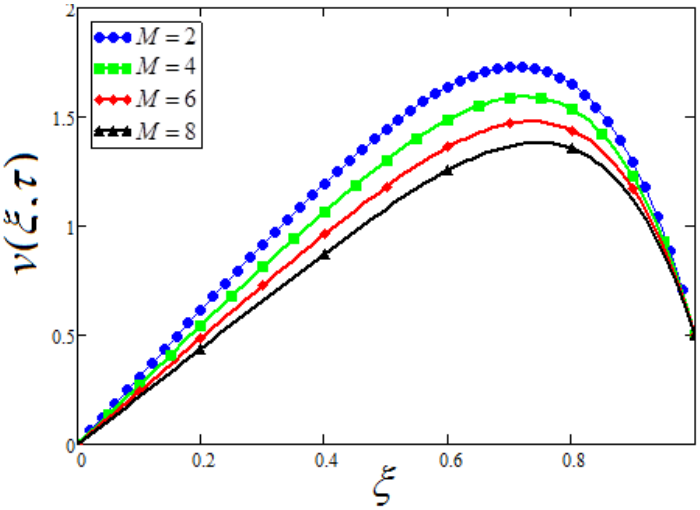

Figure 12. Variation in velocity profile for different values of M when $\lambda_1 = 0.5, \alpha = 0.2, \mathrm{P}e = 0.2, Gr = Gm = 5, \tau = 1,\ \phi = 0.02, \lambda = 1.5$.

8. Conclusions

The unsteady flow of generalized Jeffrey nanofluid in a channel is analyzed in this study. The model is generalized using the concept of Atangana–Baleanu fractional derivatives and then solved for exact solutions by the Laplace transform technique. The *ZnO* nanoparticles are chosen to be dispersed in the base fluid which is chosen as a concrete. The applications of these nanoparticles are presented in the cement industry with theoretical results. The key findings of the study are:

- ❖ The velocity profile shows that by increasing the volume fraction of the nanoparticles, the fluid becomes more viscous and as a result, the concrete will be denser and hence will be stronger.
- ❖ The concrete will be stronger for lesser values of *Gr*, as the lesser values of *Gr* reduces the velocity profile, because of the higher viscous forces and weaker thermal forces.
- ❖ Also, suspended nanoparticles in cement-concrete skin friction increase 15.26% which shows that increasing the binding strength of cement slurry and aging resistance.

Author Contributions: Conceptualization, I.K., D.L.C.C. and N.A.S.; methodology, I.K.; validation, D.L.C.C., A.A. and N.A.S.; formal analysis, N.A.S. and S.A.; investigation, I.K. and D.L.C.C.; resources, I.K. and D.L.C.C.; writing—original draft preparation, N.A.S., A.A. and S.A.; writing-review and editing, D.L.C.C. and I.K.; visualization, N.A.S.; supervision, D.L.C.C. and I.K.; project administration, I.K.; funding acquisition, D.L.C.C. All authors have read and agreed to the published version of the manuscript.

Funding: The APC was funded by CRG 015MC0 -011.

Acknowledgments: Authors acknowledge the financial support of Universiti Teknologi PETRONAS through project number CRG 015MC0 -011.

Conflicts of Interest: The authors declare no conflict of interest.

Nomenclature

$\mathrm{R_a} = \frac{\rho d U_0}{\mu}$	Reynolds number	λ_2	Jeffrey fluid parameter
$Pe = \frac{(\rho c_p)_f d U_0}{k_f}$	Peclet number	μ_{nf}	dynamic viscosity
$\lambda = \frac{\lambda_2 U_0}{d}$	Jeffrey fluid parameter	σ_{nf}	electrical conductivity
$Sc = \frac{d U_0}{D_f}$	Schmidt number	B_0	applied magnetic field
$\mathrm{M} = \frac{\sigma {B_0}^2 d}{\rho U_0}$	Hartmann number	g	gravitational acceleration
$Gr = \frac{g \beta_T d (T_w - T_0)}{{U_0}^2}$	thermal Grashof number	$(\beta_T)_{nf}$	thermal expansion
$Gm = \frac{g \beta_C d (C_w - C_0)}{{U_0}^2}$	mass Grashof number	$(\beta_C)_{nf}$	mass expansion
ρ_{nf}	density		

References

1. Whitaker, R.H.; Brann, R. Mineral Composition. Patent US7651559B2, 26 January 2010.
2. Roco, M.C.; Williams, R.S.; Alivisatos, P. *Nanotechnology Research Directions: IWGN Workshop Report. Vision for Nanotechnology R&D in the Next Decade*; National Science and Technology Council: Arlington, VA, USA, 1999.
3. Sobolev, K.; Flores, I.; Torres-Martinez, L.; Valdez, P.; Zarazua, E.; Cuellar, E. Engineering of SiO 2 nanoparticles for optimal performance in nano cement-based materials. In *Nanotechnology in Construction 3*; Springer: Berlin/Heidelberg, Germany, 2009; pp. 139–148.
4. Gann, D. A review of nanotechnology and its potential applications for construction. *SPRU Univ. Sussex* **2002**, *2002*, 28.
5. Bartos, P.J. Nanotechnology in construction: A roadmap for development. In *Nanotechnology in Construction 3*; Springer: Berlin/Heidelberg, Germany, 2009; pp. 15–26.
6. Sobolev, K.; Flores, I.; Hermosillo, R.; Torres-Martínez, L. Nanomaterials and nanotechnology for high-performance cement composites. Presented at the Presented at the ACI Session on Nanotechnology of Concrete: Recent Developments Future Perspectives, Denver, CO, USA, 7 November 2006.
7. Sobolev, K.; Gutiérrez, M.F. How nanotechnology can change the concrete world. *Am. Ceram. Soc. Bull.* **2005**, *84*, 14.

8. Zaki, S.; Ragab, K.S. How nanotechnology can change concrete industry. In Proceedings of the "1st International Conference" Sustainable Built Environment Infrastructures in Developing Countries, Bandung, Indonesia, 2–3 November 2009; p. 2170-0095.
9. Hadi, A.A.A. Nanoparticles concentration and environmental effects on cogeneration system in cement industry. *Int. J. Eng. Res. Gen. Sci.* **2015**, *3*, 786–798.
10. Nazari, A.; Riahi, S.; Riahi, S.; Shamekhi, S.F.; Khademno, A. Influence of Al2O3 nanoparticles on the compressive strength and workability of blended concrete. *J. Am. Sci.* **2010**, *6*, 6–9.
11. Morsy, M.; Alsayed, S.; Aqel, M. Hybrid effect of carbon nanotube and nano-clay on physico-mechanical properties of cement mortar. *Constr. Build. Mater.* **2011**, *25*, 145–149. [CrossRef]
12. Malhotra, V.M.; Mehta, P.K. *High-Performance, High-Volume Fly Ash Concrete: Materials, Mixture Proportioning, Properties, Construction Practice, and Case Histories*; Supplementary Cementing Materials for Sustainable Development: Ottawa, ON, Canada, 2002.
13. Raki, L.; Beaudoin, J.; Alizadeh, R.; Makar, J.; Sato, T. Cement and concrete nanoscience and nanotechnology. *Materials* **2010**, *3*, 918–942. [CrossRef]
14. Bahmani, S.H.; Huat, B.B.; Asadi, A.; Farzadnia, N. Stabilization of residual soil using SiO2 nanoparticles and cement. *Constr. Build. Mater.* **2014**, *64*, 350–359. [CrossRef]
15. Shekari, A.; Razzaghi, M. Influence of nano particles on durability and mechanical properties of high performance concrete. *Procedia Eng.* **2011**, *14*, 3036–3041. [CrossRef]
16. Givi, A.N.; Rashid, S.A.; Aziz, F.N.A.; Salleh, M.A.M. Experimental investigation of the size effects of SiO2 nano-particles on the mechanical properties of binary blended concrete. *Compos. Part B Eng.* **2010**, *41*, 673–677. [CrossRef]
17. Kang, S.; Hong, S.I.; Choe, C.R.; Park, M.; Rim, S.; Kim, J. Preparation and characterization of epoxy composites filled with functionalized nanosilica particles obtained via sol–gel process. *Polymer* **2001**, *42*, 879–887. [CrossRef]
18. Edelstein, A.S.; Cammaratra, R. *Nanomaterials: Synthesis, Properties and Applications*; CRC Press: Boca Raton, FL, USA, 1998.
19. Sobolev, K. Mechano-chemical modification of cement with high volumes of blast furnace slag. *Cem. Concr. Compos.* **2005**, *27*, 848–853. [CrossRef]
20. Sobolev, K. Effect of complex admixtures on cement properties and the development of a test procedure for the evaluation of high-strength cements. *Adv. Cem. Res.* **2003**, *15*, 67–76. [CrossRef]
21. Li, G. Properties of high-volume fly ash concrete incorporating nano-SiO2. *Cem. Concr. Res.* **2004**, *34*, 1043–1049. [CrossRef]
22. Goodarzi, M.; Safaei, M.R.; Vafai, K.; Ahmadi, G.; Dahari, M.; Kazi, S.N.; Jomhari, N. Investigation of nanofluid mixed convection in a shallow cavity using a two-phase mixture model. *Int. J. Therm. Sci.* **2014**, *75*, 204–220. [CrossRef]
23. Arasteh, H.; Mashayekhi, R.; Goodarzi, M.; Motaharpour, S.H.; Dahari, M.; Toghraie, D. Heat and fluid flow analysis of metal foam embedded in a double-layered sinusoidal heat sink under local thermal non-equilibrium condition using nanofluid. *J. Therm. Anal. Calorim.* **2019**, *138*, 1461–1476. [CrossRef]
24. Yousefzadeh, S.; Rajabi, H.; Ghajari, N.; Sarafraz, M.M.; Akbari, O.A.; Goodarzi, M. Numerical investigation of mixed convection heat transfer behavior of nanofluid in a cavity with different heat transfer areas. *J. Therm. Anal. Calorim.* **2019**, 1–25. [CrossRef]
25. Ahmadi, M.H.; Mohseni-Gharyehsafa, B.; Ghazvini, M.; Goodarzi, M.; Jilte, R.D.; Kumar, R. Comparing various machine learning approaches in modeling the dynamic viscosity of CuO/water nanofluid. *J. Therm. Anal. Calorim.* **2019**, 1–15. [CrossRef]
26. Maleki, H.; Safaei, M.R.; Togun, H.; Dahari, M. Heat transfer and fluid flow of pseudo-plastic nanofluid over a moving permeable plate with viscous dissipation and heat absorption/generation. *J. Therm. Anal. Calorim.* **2019**, *135*, 1643–1654. [CrossRef]
27. Safaei, M.R.; Togun, H.; Vafai, K.; Kazi, S.N.; Badarudin, A. Investigation of heat transfer enhancement in a forward-facing contracting channel using FMWCNT nanofluids. *Numer. Heat Transf. Part A Appl.* **2014**, *66*, 1321–1340. [CrossRef]
28. Gholamalizadeh, E.; Pahlevanzadeh, F.; Ghani, K.; Karimipour, A.; Nguyen, T.K.; Safaei, M.R. Simulation of water/FMWCNT nanofluid forced convection in a microchannel filled with porous material under slip velocity and temperature jump boundary conditions. *Int. J. Numer. Methods Heat Fluid Flow* **2019**. [CrossRef]

29. Jalali, E.; Ali Akbari, O.; Sarafraz, M.M.; Abbas, T.; Safaei, M.R. Heat transfer of oil/MWCNT nanofluid jet injection inside a rectangular microchannel. *Symmetry* **2019**, *11*, 757. [CrossRef]
30. Bahiraei, M.; Jamshidmofid, M.; Goodarzi, M. Efficacy of a hybrid nanofluid in a new microchannel heat sink equipped with both secondary channels and ribs. *J. Mol. Liq.* **2019**, *273*, 88–98. [CrossRef]
31. Giwa, S.O.; Sharifpur, M.; Goodarzi, M.; Alsulami, H.; Meyer, J.P. Influence of base fluid, temperature, and concentration on the thermophysical properties of hybrid nanofluids of alumina–ferrofluid: Experimental data, modeling through enhanced ANN, ANFIS, and curve fitting. *J. Therm. Anal. Calorim.* **2020**, 1–19. [CrossRef]
32. Peng, Y.; Zahedidastjerdi, A.; Abdollahi, A.; Amindoust, A.; Bahrami, M.; Karimipour, A.; Goodarzi, M. Investigation of energy performance in a U-shaped evacuated solar tube collector using oxide added nanoparticles through the emitter, absorber and transmittal environments via discrete ordinates radiation method. *J. Therm. Anal. Calorim.* **2020**, *139*, 2623–2631. [CrossRef]
33. Sarafraz, M.M.; Dareh Baghi, A.; Safaei, M.R.; Leon, A.S.; Ghomashchi, R.; Goodarzi, M.; Lin, C.-X. Assessment of Iron Oxide (III)–Therminol 66 Nanofluid as a Novel Working Fluid in a Convective Radiator Heating System for Buildings. *Energies* **2019**, *12*, 4327. [CrossRef]
34. Karimipour, A.; Bagherzadeh, S.A.; Taghipour, A.; Abdollahi, A.; Safaei, M.R. A novel nonlinear regression model of SVR as a substitute for ANN to predict conductivity of MWCNT-CuO/water hybrid nanofluid based on empirical data. *Phys. A Stat. Mech. Its Appl.* **2019**, *521*, 89–97. [CrossRef]
35. Maleki, H.; Safaei, M.R.; Alrashed, A.A.A.A.; Kasaeian, A. Flow and heat transfer in non-Newtonian nanofluids over porous surfaces. *J. Therm. Anal. Calorim.* **2019**, *135*, 1655–1666. [CrossRef]
36. Özgür, Ü.; Alivov, Y.I.; Liu, C.; Teke, A.; Reshchikov, M.; Doğan, S.; Avrutin, V.; Cho, S.-J.; Morkoç, H. A comprehensive review of ZnO materials and devices. *J. Appl. Phys.* **2005**, *98*, 11. [CrossRef]
37. Bhattacharyya, S.; Gedanken, A. A template-free, sonochemical route to porous ZnO nano-disks. *Microporous Mesoporous Mater.* **2008**, *110*, 553–559. [CrossRef]
38. Ludi, B.; Niederberger, M. Zinc oxide nanoparticles: Chemical mechanisms and classical and non-classical crystallization. *Dalton Trans.* **2013**, *42*, 12554–12568. [CrossRef]
39. Nochaiya, T.; Sekine, Y.; Choopun, S.; Chaipanich, A. Microstructure, characterizations, functionality and compressive strength of cement-based materials using zinc oxide nanoparticles as an additive. *J. Alloys Compd.* **2015**, *630*, 1–10. [CrossRef]
40. Arefi, M.R.; Rezaei-Zarchi, S. Synthesis of zinc oxide nanoparticles and their effect on the compressive strength and setting time of self-compacted concrete paste as cementitious composites. *Int. J. Mol. Sci.* **2012**, *13*, 4340–4350. [CrossRef] [PubMed]
41. Flores-Velez, L.M.; Dominguez, O. Characterization and properties of Portland cement composites incorporating zinc-iron oxide nanoparticles. *J. Mater. Sci.* **2002**, *37*, 983–988. [CrossRef]
42. Taylor-Lange, S.C.; Riding, K.A.; Juenger, M.C. Increasing the reactivity of metakaolin-cement blends using zinc oxide. *Cem. Concr. Compos.* **2012**, *34*, 835–847. [CrossRef]
43. Nguyen, T.M.T.; Wang, P.-W.; Hsu, H.-M.; Cheng, F.-Y.; Shieh, D.-B.; Wong, T.-Y.; Chang, H.-J. Dental cement' biological and mechanical properties improved by ZnO nanospheres. *Mater. Sci. Eng. C* **2019**, *97*, 116–123. [CrossRef]
44. Gowda, R.; Narendra, H.; Mourougane, R.; Nagabhushana, B. Performance of Nano-SiO 2 and Nano-ZnO 2 on Compressive Strength and Microstructure Characteristics of Cement Mortar. In *Sustainable Construction and Building Materials*; Springer: Berlin/Heidelberg, Germany, 2019; pp. 13–22.
45. Atangana, A.; Baleanu, D. New fractional derivatives with nonlocal and non-singular kernel: Theory and application to heat transfer model. *Therm. Sci.* **2016**, *20*, 763–769. [CrossRef]
46. Atangana, A.; Koca, I. Chaos in a simple nonlinear system with Atangana–Baleanu derivatives with fractional order. *Chaos Solitons Fractals* **2016**, *89*, 447–454. [CrossRef]
47. Ali, F.; Sheikh, N.A.; Khan, I.; Saqib, M. Magnetic field effect on blood flow of Casson fluid in axisymmetric cylindrical tube: A fractional model. *J. Magn. Magn. Mater.* **2017**, *423*, 327–336. [CrossRef]
48. Khan, A.; Khan, D.; Khan, I.; Taj, M.; Ullah, I.; Aldawsari, A.M.; Thounthong, P.; Sooppy Nisar, K. MHD Flow and Heat Transfer in Sodium Alginate Fluid with Thermal Radiation and Porosity Effects: Fractional Model of Atangana–Baleanu Derivative of Non-Local and Non-Singular Kernel. *Symmetry* **2019**, *11*, 1295. [CrossRef]

49. Sheikh, N.A.; Ali, F.; Saqib, M.; Khan, I.; Jan, S.A.A. A comparative study of Atangana-Baleanu and Caputo-Fabrizio fractional derivatives to the convective flow of a generalized Casson fluid. *Eur. Phys. J. Plus* **2017**, *132*, 54. [CrossRef]
50. Sheikh, N.A.; Ali, F.; Saqib, M.; Khan, I.; Jan, S.A.A.; Alshomrani, A.S.; Alghamdi, M.S. Comparison and analysis of the Atangana–Baleanu and Caputo–Fabrizio fractional derivatives for generalized Casson fluid model with heat generation and chemical reaction. *Results Phys.* **2017**, *7*, 789–800. [CrossRef]
51. Sheikh, N.A.; Ali, F.; Khan, I.; Gohar, M.; Saqib, M. On the applications of nanofluids to enhance the performance of solar collectors: A comparative analysis of Atangana-Baleanu and Caputo-Fabrizio fractional models. *Eur. Phys. J. Plus* **2017**, *132*, 540. [CrossRef]
52. Asif, M.; Ul Haq, S.; Islam, S.; Abdullah Alkanhal, T.; Khan, Z.A.; Khan, I.; Nisar, K.S. Unsteady Flow of Fractional Fluid between Two Parallel Walls with Arbitrary Wall Shear Stress Using Caputo–Fabrizio Derivative. *Symmetry* **2019**, *11*, 449. [CrossRef]
53. Gohar, M.; Ali, F.; Khan, I.; Sheikh, N.A.; Shah, A. The unsteady flow of generalized hybrid nanofluids: Applications in cementitious materials. *J. Aust. Ceram. Soc.* **2018**, *55*, 657–666. [CrossRef]
54. Atangana, A.; Koca, I. New direction in fractional differentiation. *Math. Nat. Sci.* **2017**, *1*, 18–25. [CrossRef]
55. Sheikh, N.A.; Ali, F.; Khan, I.; Gohar, M. A theoretical study on the performance of a solar collector using CeO2 and Al2O3 water based nanofluids with inclined plate: Atangana–Baleanu fractional model. *ChaosSolitons Fractals* **2018**, *115*, 135–142. [CrossRef]
56. Vieru, D.; Fetecau, C.; Fetecau, C. Flow of a viscoelastic fluid with the fractional Maxwell model between two side walls perpendicular to a plate. *Appl. Math. Comput.* **2008**, *200*, 459–464. [CrossRef]
57. Siddique, I.; Vieru, D. Exact solution for the rotational flow of a generalized second grade fluid in a circular cylinder. *Acta Mech. Sin.* **2009**, *25*, 777–785. [CrossRef]
58. Hristov, J. The non-linear Dodson diffusion equation: Approximate solutions and beyond with formalistic fractionalization. *Math. Nat. Sci.* **2017**, *1*, 1–17. [CrossRef]
59. Atangana, A.; Bildik, N. The use of fractional order derivative to predict the groundwater flow. *Math. Probl. Eng.* **2013**, *2013*, 543026. [CrossRef]
60. Besbes, S.D.; Guillopé, C. Non-isothermal flows of viscoelastic incompressible fluids. *Nonlinear Anal.* **2001**, *44*, 919–942. [CrossRef]
61. Djabi, A.; Merouani, A.; Aissaoui, A. A frictional contact problem with wear involving elastic-viscoplastic materials with damage and thermal effects. *Electron. J. Qual. Theory Differ. Equ.* **2015**, *2015*, 1–18. [CrossRef]
62. Kothandapani, M.; Srinivas, S. Peristaltic transport of a Jeffrey fluid under the effect of magnetic field in an asymmetric channel. *Int. J. Non-Linear Mech.* **2008**, *43*, 915–924. [CrossRef]
63. Artemov, M.A.; Baranovskii, E.S. Solvability of the Boussinesq Approximation for Water Polymer Solutions. *Mathematics* **2019**, *7*, 611. [CrossRef]
64. Ali, F.; Gohar, M.; Khan, I. MHD flow of water-based Brinkman type nanofluid over a vertical plate embedded in a porous medium with variable surface velocity, temperature and concentration. *J. Mol. Liq.* **2016**, *223*, 412–419. [CrossRef]
65. Zakian, V. Numerical inversion of Laplace transform. *Electron. Lett.* **1969**, *5*, 120–121. [CrossRef]
66. Reches, Y. Nanoparticles as concrete additives: Review and perspectives. *Constr. Build. Mater.* **2018**, *175*, 483–495. [CrossRef]